Chemical Physics Letters 787 (2022) 139229

Contents lists available at ScienceDirect

Chemical Physics Letters

journal homepage: www.elsevier.com/locate/cplett

Growth pattern of doubly metal doped silicon clusters M_2Si_n with M_2 = Mo_2, Nb_2, Ta_2, W_2, NbMo, TaW and n = 11–18. Formation of fused cages M_2Si_{18}

Hung Tan Pham [a,*], Cam-Tu Phan Dang [b], Long Van Duong [a], Phan Toai Tuyn [a], Minh Tho Nguyen [a,c,*]

[a] Institute for Computational Science and Technology (ICST), Ho Chi Minh City, Viet Nam
[b] Department of Chemistry, Faculty of Natural Sciences, Quy Nhon University, Quy Nhon, Viet Nam
[c] Department of Chemistry, KU Leuven, B-3001 Leuven, Belgium

ARTICLE INFO

Keywords:
Silicon clusters
Doubly metal doped silicon clusters
M_2Si_{18} fused cage clusters
Electron shell
Density functional theory

ABSTRACT

Geometries of doubly transition metal doped silicon clusters M_2Si_n, M_2 = Mo_2, Nb_2, Ta_2, W_2, NbMo, TaW were determined by DFT computations. Geometries of M_2Si_n in the range from 11 to 18 Si atoms change from a tubular shape to a cage and then a fused cage. The M_2Si_{18} sizes present us with a novel structural motif, the fused cage, for silicon clusters. Such fused cages arise from a fusion of both MSi_{10} and MSi_{12} prisms followed by addition of two Si atoms. Formation and filling of electron shells contribute to the high thermodynamic stability of M_2Si_{18} fused clusters.

1. Introduction

The silicon element has long been known to be essential for semiconductor and optoelectronic industries [1–4]. The continuous trend of miniaturization in microelectronics triggers a quest for new nanostructured building blocks. Therefore, there has been tremendous interest in novel Si clusters that can be used as assemblies [5–13]. The doping of transition metal atoms into a Si host has been known as an efficient approach to generate high symmetry and stability derivatives that are suitable for cluster-assembled materials. The most popular examples include the twelve Si atoms clusters doped by a variety transition metals [14–19]. A common feature of these structures is having one metal dopant centered in a Si_{12} hexagonal prism. The existence of the MSi_{16} Frank-Kasper cluster, a structure in which sixteen Si atoms establish a T_d cage and completely encapsulate the metal atom M, emphasizes a particular effect of the transition metal dopants in producing high symmetry structure [20,21]. Previous studies predicted that both MSi_{12} hexagonal prisms and MSi_{16} Frank-Kasper structures are suitable for cluster-assembled materials. For example, VSi_{12} illustrates a case in which a hexagonal prism can generate a magnetic sheet in a honeycomb-like framework [22]. The MSi_{16} structures, with M = Sc, Ti and V, were predicted to form the $ScSi_{16}$-VSi_{16} hetero-dimer and $ScSi_{16}$-$TiSi_{16}$-VSi_{16} hetero-trimer [23]. Following prediction on the formation of metallic silicon tubes, the $BeSi_{12}$ hexagonal prismatic building unit was used to constructed the $[BeSi_{12}]_n$ nanotube [24]. Hence, the search for silicon clusters doped by transition metals continues to be highly important in the development of novel materials, as they provide us with a wide range of potential building blocks with non-classical shapes and properties.

The prismatic/anti-prismatic dual motifs of doped silicon clusters are special because they are considered as embryo for formation of nanotubes. Twelve Si atoms clusters doped by two and three dopants were found to be stable in tubular shape. Exploration on the series $M_2Si_{12}^q$ with M_2 = Nb_2, Ta_2, Mo_2, W_2, NbMo and TaW, q = −2, 0, +2 pointed out the dominance of tubular structure constructed by two Si_6 strings [24,25]. Computed results showed two different structural motifs that emerge as the global energy minima of such clusters. They are basically singlet tubes with either a C_{2v} prism ($^1A_1$) or a C_{6v} antiprism ($^1A_1$) forms. The anion $V_3Si_{12}^-$ presents us with a particular structure in which three V atoms having a linear V-V-V form are placed inside a (2 × 6) hexagonal anti-prism Si_{12} [26]. Also the twelve Si atom clusters such as B_2Si_{12} and $B_3Si_{12}^+$ yield stable isomers in which both B_2 and B_3 units are encapsulated by Si_{12} (2 × 6) hexagonal prisms [27]. Particularly, within the $B_3Si_{12}^+$ tube, the B_3 cycle is not only encapsulated by a Si_{12} prism but

* Corresponding authors.
E-mail addresses: hung.pt@icst.org.vn (H.T. Pham), minh.nguyen@kuleuven.be (M.T. Nguyen).

https://doi.org/10.1016/j.cplett.2021.139229
Received 14 August 2021; Received in revised form 10 November 2021; Accepted 14 November 2021
Available online 16 November 2021

also tunes its aromatic feature. A similar formation is also identified for $B_3Ge_{12}^+$ and B_4Ge_{12} where the Ge_{12} hexagonal prism is centered by a B_3 and B_4 cycle, respectively [28]. Doping using a small boron cluster emerges as an efficient approach to generate high symmetry stabilized structure for both silicon and germanium clusters. Of the tubular clusters, a special case is the Mn_2Si_{15} triple ring which is stable in a tubular form whose three Si_5 strings are joint in anti-prism fashion, and the dimer Mn_2 is vertically placed inside the Si tube [29]. The appearance of Mn_2Si_{15} suggests that triple ring structures likely appear upon doping of two transition metals along the increasing Si_n sizes.

The above brief summary points out that the use of various dopants going from transition metals to small boron cycles helps generating a tubular structure constructed by joining two Si_6 strings for cases of hexagonal prism/anti-prism, and three Si_5 strings as in case of Mn_2Si_{15}. Accordingly, the M_2Si_{18} clusters could be predicted to be the next tubular shape constructed by superposition of three Si_6 strings. Although the formation capacity of tubular shape has been examined for the eighteen Si atoms cluster doped by two *3d*-metals (from Ti to Zn) [30], no exploration on *4d* or *5d* metals is available yet. It is thus of interest to explore the geometries of the M_2Si_{18} clusters with M being a *4d* or *5d* metal. In addition, the existence of M_2Si_{12} tubular clusters with M_2 = Nb_2, Mo_2, NbMo, Ta_2, W_2, TaW shows that these dopants can stabilize a silicon host into a tubular shape. Therefore, we set out to systematically determine the geometries of M_2Si_n clusters with the same series of dopants M_2 = Nb_2, Mo_2, NbMo, Ta_2, W_2, TaW, and the Si cluster sizes ranging from 11 to 18. As a result, the M_2Si_{18} clusters are found to feature a fused cluster rather than a triple ring tube. Moreover, we would probe further a structural transition from a tubular shape through a cage form to a fused cage in this series of M_2Si_n clusters

2. Computational methods

In order to identify the geometries of M_2Si_n clusters we use a stochastic genetic algorithm developed earlier by us [31]. We now modify this algorithm by adding a permutation subroutine in which each atom exchanges its position with all the others. Moreover, to ensure that the global energy minimum isomer of each size is correctly found, several series of geometries having non-conventional shapes are also considered with the aim to search for unexpectedly stable structures. We use density functional theory (DFT) with the hybrid B3P86 functional [32,33] for initial geometry optimizations in view of previous results that this functionals provides reliable results for Si clusters [34]. Initial structures are first optimized using the small 3-21G and 3-21G(d) basis sets [35,36]. The optimized isomers whose relative energies are lying within a range of 50 kcal/mol with respect to the lowest-lying one, are subsequently reoptimized using the same functional, but in conjunction with the larger 6-311+G(d) basis set for Si atom and aug-cc-pVTZ–PP for metal elements [37,38]. Due to the presence of transition metals that could exist in high spin states, these isomers are geometrically optimized in different spin states with the aim to identify the ground electronic state of each cluster considered. Harmonic vibrational frequencies are analyzed afterwards at the same level to ensure the character of optimized structures as local energy minima and to estimate their zero-point energies (ZPE). To probe the chemical bonding of the clusters considered, their electron densities are determined by mean of NBO atomic charges [39]. All standard electronic structure theory computations are performed using the Gaussian 09 suite of program [40].

3. Results and discussion

3.1. Geometrical features

As for a convention, isomers discussed hereafter are labelled by **M2.n.x** and **MM.n.x** in which **M** is the transition metal considered, **n** being the number of Si atoms and × = **A**, **B**, **C**… denoting the isomers with increasing relative energy. Thus, **M2.n.A** or **MM.n.A** invariably refers to the lowest-lying isomer and the relative energy reference of the relevant system.

M_2Si_{11}, M_2Si_{12} and M_2Si_{13}. Fig. 1 displays the geometric shapes of the most stable isomers of Mo_2Si_n, $NbMoSi_n$, Nb_2Si_n, W_2Si_n, $TaWSi_n$ and Ta_2Si_n with sizes of n = 11, 12 and 13. Their lower-lying isomers are given in Figs. S1, S2, S3 and S4 of the Electronic Supplementary Information (ESI) file. Both M_2Si_{11} and M_2Si_{13} are formed on the basis of M_2Si_{12} tubular structures [31]. Our results on M_2Si_{12} are similar to previous reports in which Nb_2Si_{12} and Ta_2Si_{12} are hexagonal prisms whereas Mo_2Si_{12} and W_2Si_{12} are rather stable in hexagonal antiprism.

Both **Nb2.11.A** and **Nb2.11.B** are energetically degenerate isomers with a meaningless separation energy of only 0.05 kcal/mol. These structures are formed by removal of one Si atom of **Nb2.12.A** and **Nb2.12.B**, respectively. Similarly, removal of one Si atom of **Mo2.12.A** generates for Mo_2Si_{11} four lowest-energy isomers including **Mo2.11.A**, **Mo2.11.B**, **Mo2.11.C** and **Mo2.D**. **NbMo.11.A** is a hexagonal antiprism containing one defect site. The **Ta2.11.B**, **Ta2.11.C** and **Ta2.11.D** isomers are only ~ 2 kcal/mol less stable and thus competitive for the ground state with **Ta2.11.A**. Regarding the W_2Si_{11} cluster, **W2.11.A** is also formed by removing one Si atom of W_2Si_{12} hexagonal anti-prism, whereas the mixed **TaW.11.A** is a defected tube.

For their part, each M_2Si_{13} is generated by addition of one Si atom to the M_2Si_{12} tube. **Nb2.13.A**, **Ta2.13.A, Mo2.13.A** and **W2.13.A** come from the corresponding M_2Si_{12} antiprisms. Both mixed $NbMoSi_{13}$ and $TaWSi_{13}$ clusters are equally stable in the same shape (Fig. 1).

M_2Si_{14}, M_2Si_{15} and M_2Si_{16}: competition between tube and cage. The most stable isomers of M_2Si_{14}, M_2Si_{15} and M_2Si_{16} are shown in Fig. 2, whereas their lower-lying isomers are given in Figs. S6, S7 and S8 of the ESI file. Both Nb_2Si_{14} and Ta_2Si_{14} clusters are stable in cage structures in which only one metal atom is completely covered by a Si_{14} cage, and the other metal is coordinated to a pentagonal face of the Si_{14} cage. Mo_2Si_{14} and W_2Si_{14} prefer to form tubes upon addition of two Si atoms into Mo_2Si_{12} and W_2Si_{12} hexagonal prisms. The isomers **Mo2.14.A**, **Mo2.14.B** and **Mo2.14.C** are produced by adding two Si atoms into Mo_2Si_{12} at various positions. Their energy difference is only ~2 kcal/mol making them the quasi-degenerate ground state. Similarly, injection of two Si atoms into W_2Si_{12} at various sites generates both **W2.14.A** and **W2.14.B** in which the latter is only 3 kcal/mol higher.

For the mixed $NbMoSi_{14}$, within **NbMo.14.A** the Mo dopant is enclosed by a Si_{14} cage but Nb atom is capped to a pentagonal face. The next isomer **NbMo.14.B** has a tubular shape and lies only 1.5 kcal/mol above.. This structure is generated by adding two Si atoms into the **NbMo.12.B** prism. Regarding the other mixed $TaWSi_{14}$, both tubular **TaW.14.A** and **TaW.14.B** isomers are produced from **TaW.12.B** and energetically quasi-degenerate.

The Nb_2Si_{15} and Ta_2Si_{15} clusters are stabilized in a similar geometry. **Nb2.15.A** and **Ta2.15.A** are produced from the lower size following the same growth pattern. In the hetero-doped cages, **NbMo.15.A** and **TaW.15.A** are again characterized by a comparable shape in which either Mo or W atom is located inside, and Nb or Ta is attached at an *exo*-position. DFT calculations point out that in the stable cage **Mo2.15.A**, one Mo atom is enclosed by a Si_{14} cage, but the other Mo interacts with a pentagonal face, and the last Si atom is bonded to an Si-Si edge of the Si_{14} cage. **W2.15.A** is found in a slightly different form in which one W atom is covered by a smaller Si_{13} cage, the second W is situated outside, and the last two Si atoms are capped on an Si-Si edge.

Within **Nb.16.A**, one Nb atom is put inside an Si_{15} cage, and the other is coordinated to an Si_5 pentagonal face, and one Si atom is now attached to a triagonal Si_3 face of the Si_{15} cage. **Nb.16.B** is a tube-based structure and lies only 2.5 kcal/mol above, and thus competitive for the ground state status of $Nb_2@Si_{16}$.

Both lowest-lying **Ta2.16.A** and **Ta2.16.B** have a cage-like shape and a separation energy of ~3 kcal/mol. In **Ta2.16.A**, one Ta atom is covered by a Si_{14} cage, the second Ta is complexed with a Si_5 pentagonal face, along with two Si atoms attached to the Si_{14} cage. In the **Ta2.16.B** cage, the last Si atom interacts with a triangular Si_3 face of a Ta_2Si_{15}

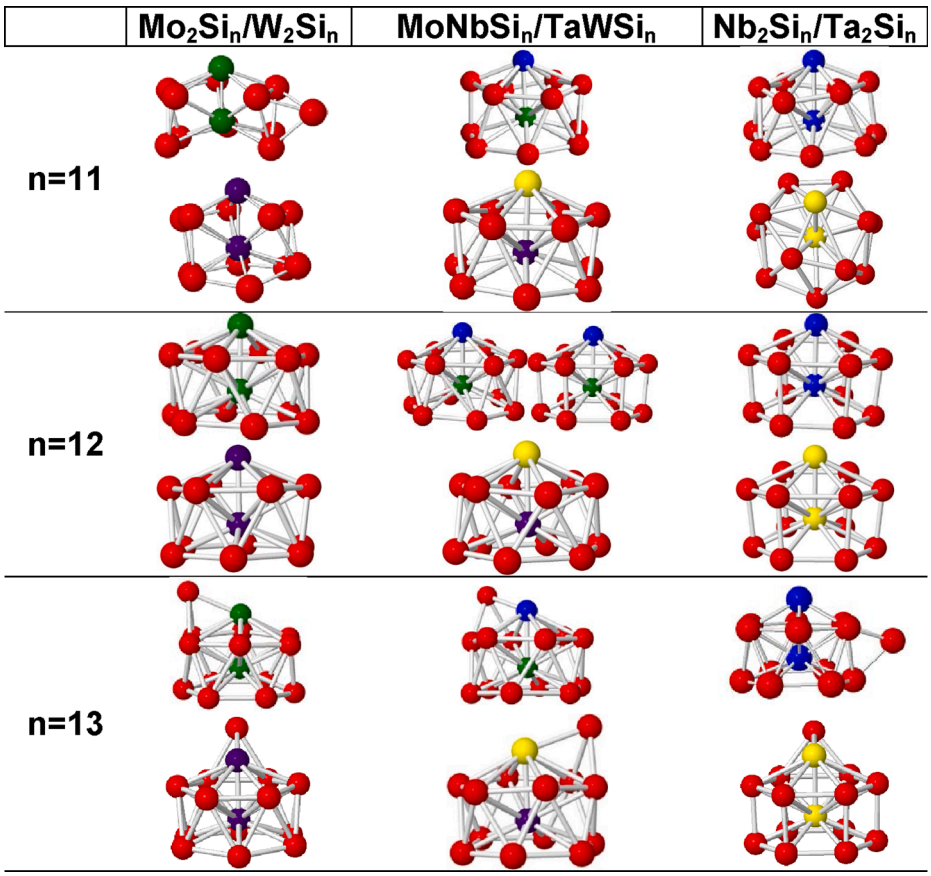

Fig. 1. The most stable isomer of each M_2Si_n cluster with M_2 = Nb_2, NbMo, Mo_2, W_2, TaW and Ta_2 and n = 11–13. Geometry optimizations and energy calculations were performed using the B3P86 functional with the 6–311 + G(d) basis set for Si and aug-cc-pVTZ-PP for metal atoms.

cage. It is interesting that Mo_2Si_{16} tends to favour formation of a tube over a cage. In fact **Mo2.16.A** features as a defected triple ring in which two Si_6 strings and one Si_4 ring connect together. The tungsten W_2Si_{16} cluster prefers a cage rather than a tube, in contrast to its isovalent Mo_2Si_{16}. In **W2.16.A** one W is again placed at an exohedral position and the other is completely situated inside a Si_{16} cage.

Of the mixed clusters, **NbMo.16.A** is of tubular shape in which the first Nb atom is found inside a (6x2) Si_{12} hexagonal prism, and Mo atom is fixed on a hexagonal face, and the 4 last Si atoms are attached to a Si_6 ring along the Nb-Mo axis making the third ring for the Si_{16} host. On the contrary, $TaWSi_{16}$ favours a stabilized cage. The isomers **TaW.16.A**, **TaW.16.B**, **TaW.16.C**, **TaW.16.D** and **TaW.16.D** are very close in energy, with a separation energy of only ~2.5 kcal/mol. Within all these lower-lying structures, W sits completely inside the Si cage whereas Ta prefers to be placed outside.

M_2Si_{17} and M_2Si_{18}: Formation of fused cages. Results on geometric identification of both sizes are given in Fig. 3 and Figs. S8 and S9 of the ESI file. Within the **Nb.17.A** cage, the same feature emerges concerning the positions of both Nb dopants. The tubular isomer **Nb2.17.B** is much less stable. In contrast, both isomers **Ta2.17.A** and **Ta2.17.B** are separated by a small energy gap of ~ 1.5 kcal/mol. In both structures, one Ta dopant remains at an exohedral position, showing that the Si_{17} size is still not large enough to completely encapsulate two Ta or Nb dopants.

Both Mo_2Si_{17} and W_2Si_{17} clusters present a novel type of structural motif, namely, **Mo2.17.A** features as a peculiar fusion of both the $MoSi_{14}$ cage and $MoSi_{12}$ prism with a removal of one Si atom of the Si_{12} prism. Similarly, **W2.17.A** is equally generated upon fusion of a WSi_{14} cage and a WSi_{12} prism. Geometric features of the hetero-doped $NbMoSi_{17}$ and $TaWSi_{17}$ show that they still prefer a cage in which only one metal, Mo or W dopant, is completely covered.

The M_2Si_{18} clusters present another novel endohedral type. In fact, in **Nb2.18.A** all 18Si atoms form a C_s polyhedral cage consisting of 2 hexagons, 4 pentagons and 3 rhombuses, and then it completely sequestrates a Nb_2 dimer. A similar endohedral cage **Ta2.18.A** is found for Ta_2Si_{18} which consists a C_s Si_{18} polyhedral cage centered by a Ta-Ta dimer.

For Mo_2Si_{18}, both lowest-lying **Mo2.18.A** and **Mo2.18.B** are close in energy by a gap of ~2 kcal/mol. **Mo2.18.B** exhibits a similar geometry as Nb_2Si_{18} and Ta_2Si_{18} in which two Mo atoms are completely centered inside a Si_{18} polyhedron. In contrast, **Mo2.18.A** is an endohedral cage generated by a structural distortion from **Mo2.18.B** without (C_1) symmetry. Both isomers **W2.18.A** and **W2.18.B** are predicted to be quasi-degenerate ground state for W_2Si_{18}, with a relative energy of ~1 kcal/mol. They both are endohedral cages with a W_2 dimer in C_1 and C_s Si_{18} polyhedra, respectively. For $NbMoSi_{18}$, both **NbMo.18.A** and **NbMo.18.B** are practically degenerate as their relative energy amounts to only ~2 kcal/mol. **NbMo.18.A** is made from a C_s Si_{18} cage consisting of 2 hexagons, 3 pentagons, 3 rhombuses and 2 triangles, and is centered by a hetero-nuclear Nb-Mo dimer. **NbMo.18.B** is an endohedral cage in which the Nb-Mo hetero-dimer lies completely inside a Si_{18} cage as in the case of **Nb2.18.A** and **Mo2.18.B**. The geometry of $TaWSi_{18}$ illustrates a predominance of fully endohedral structure in such a way that the lower-lying **TaW.18.A**, **TaW.18.B** and **TaW.18.C** isomers are quasi-degenerate ground state as their relative energy ranges within ~1 kcal/mol.

3.2. *Growth pattern of M_2Si_n clusters: From tube to fused cage*

Having established the geometrical features of the doubly doped silicon clusters in eight sizes and six combinations of dopants, we now examine their growth patterns and the factors governing them. For the

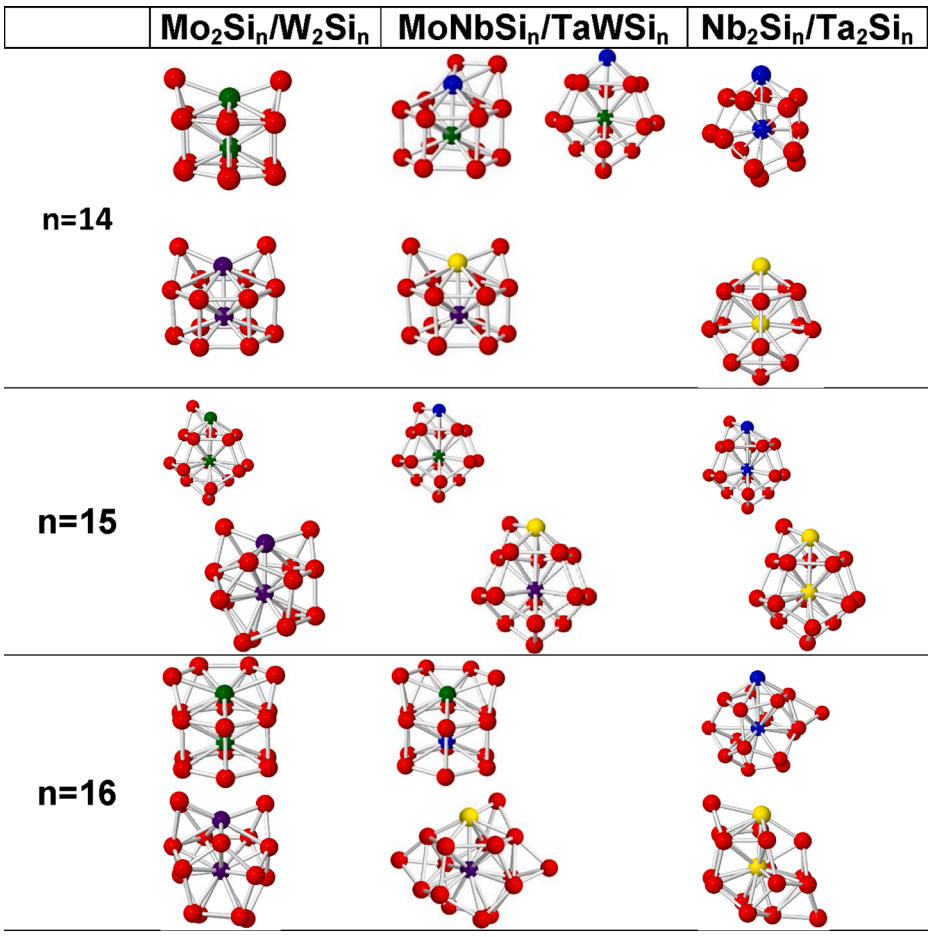

Fig. 2. The most stable isomers of M_2Si_n clusters with $M_2 = Nb_2$, NbMo, Mo_2, W_2, TaW and Ta_2 and n = 14–16. Geometry optimizations and energy calculations were performed using the B3P86 functional and the 6-311+G(d) basis set for Si and aug-cc-pVTZ-PP for metal atoms.

sake of simplicity, Fig. 4 displays only the structural growth patterns of Nb_2Si_n, Mo_2Si_n and the mixed $NbMoSi_n$ clusters with n = 11 – 18. The trends of Ta_2Si_n, W_2Si_n and $TaWSi_n$ clusters are given in Fig. S10 of the ESI file. Table 1 summarizes the shape of the lowest-lying isomer in each case.

Geometric structures of the M_2-doped silicon clusters in the range from 11 to 18 Si atoms tend to change from a tubular shape to a cage and then a fused cage. Indeed, the geometries of the smaller M_2Si_{11}, M_2Si_{12} and M_2Si_{13} clusters enjoy a predominance of a tube. While each M_2Si_{11} is consistently generated by removal of one Si atom from M_2Si_{12}, each M_2Si_{13} is produced by addition of one extra Si atom to the corresponding M_2Si_{12}. From sizes 14 to 18, the M_2Si_n geometries undergo a structural transition from a tube to a singly doped cage and then a fused cage at the size of 18 Si atoms.

The Nb_2Si_n and Ta_2Si_n series with n = 14–17 obviously prefer a cage-like configuration, which is turned out by successive addition of Si atoms to the Nb_2Si_{14} and Ta_2Si_{14}, respectively. In the size range of 14–17, Mo_2Si_n appear to fluctuate between a tube and a cage. For W_2Si_n cluster, only W_2Si_{14} is a tube whereas W_2Si_{15}, W_2Si_{16} and W_2Si_{17} all are favored in a cage construction.

Within the sizes 14–17, geometries of the hetero-metallic $NbMoSi_n$ clusters also vary between tube and cage. On the contrary, the cage shape dominates in the mixed series $TaWSi_n$. Finally, the fused cage appears and takes over in the M_2Si_{18} sizes. Regarding the position of both metal dopants, the size increase going from 11 to 18 Si atoms allows a gradual transition from an exohedral to an endohedral cage with respect to the position of both dopants.

Of the eighteen-atom clusters doped by two transition metal atoms, both polyanions $Pd_2Ge_{18}^{4-}$ and $Pd_2Sn_{18}^{4-}$ appear as the largest single deltahedron cages in which the Pd_2 dimer is fully captured by Ge_{18} and Sn_{18} deltahedral cages [41,42]. The corresponding M_2Si_{18} are characterized by two-metal-atom encapsulated polyhedrons, but their Si_{18} cages are made of hexagons, pentagons, rhombuses and triangles rather than only triangular faces such as the case in a deltahedral cage. It is highly interesting that these polyhedra generated following a similar approach; that is, they are generated by fusion of smaller clusters. As a matter of fact, while the $Pd_2Sn_{18}^{4-}$ and $Pd_2@Ge_{18}^{4-}$ deltahedra are formed by fusion of two $PdSn_{12}$ and $PdGe_{12}$ units, respectively, the M_2Si_{18} clusters arise from a fusion of both MSi_{10} and MSi_{12} prisms followed by addition of two Si atoms. The fusion pathway which generates M_2Si_{18} from both MSi_{10} plus MSi_{12} prisms is displayed in Fig. 5. A MSi_{10} pentagonal prism is actually added by two extra Si atoms along the C_s axis to produce a MSi_{14} cage. The latter cage emerges with a MSi_{12} hexagonal prism, which is the most stable isomer of MSi_{12}, via a sharing of six Si sites, and ends up with formation of a M_2Si_{18} polyhedron. Generation of a polyhedron following fusion of small cages suggests a general, and seemingly simple, route in which a large size cluster can be formed by fusing smaller clusters.

3.3. *Stability and chemical bonding of the fused M_2Si_{18} clusters*

We now attempt to rationalize the high stability of the M_2Si_{18} fused clusters. The M−M distances and NBO charges calculated for M_2Si_n clusters are given in Table 2. The M−M distances are in a range of 2.3 ~ 3.2 Å, from dimeric bonds to non-bonding. The endohedral metal dopant has an atomic NBO charge value varying in a range of −2.4 and −3.8

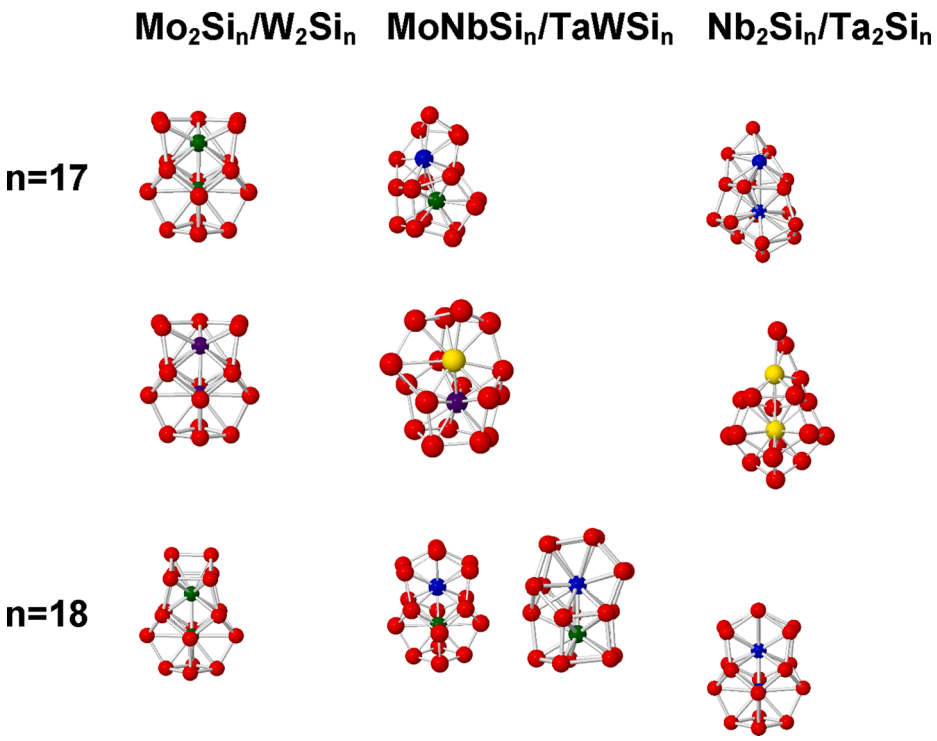

Fig. 3. The most stable isomer of M_2Si_n clusters with M_2 = Nb_2, NbMo, Mo_2, W_2, TaW and Ta_2 and n = 17–18. Geometry optimizations and energy calculations were performed using the B3P86 functional and the 6-311+G(d) basis set for Si and aug-cc-pVTZ-PP for metal atoms.

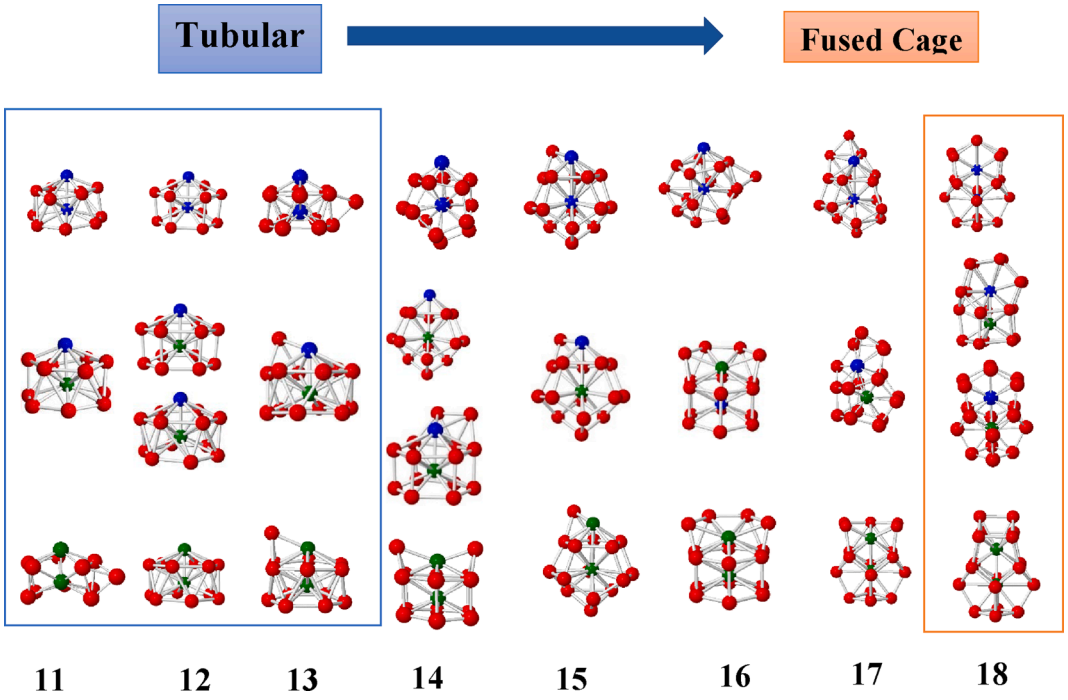

Fig. 4. The growth pattern of Nb_2Si_n, $NbMoSi_n$ and Mo_2Si_n. Higher panel is for Nb_2Si_n, middle panel $NbMoSi_n$ and lower panel Mo_2Si_n.

electron, whereas the outer metal becomes more negatively charged along with the increasing size. This result points out that Si hosts consistently give a charge transfer to metal dopants. An important consequence is that within each M_2Si_n cluster, the metal dopant turns out to be a negative island surrounded by a positively charged Si_n host in such a way that electrostatic interactions likely play a predominant role in stabilizing the corresponding M_2Si_n cluster.

Stability of silicon clusters doped by transition metal atoms was successfully rationalized by using the electron shell model, or the Jellium model [43]. Within this model, the valence electrons tend to move freely under a mean field formed core electrons and nuclei. These valence electrons occupy the S, P, D, F,… shells, defined by orbitals according to the angular momentum number L = 0, 1, 2, 3… and with a given quantum number L, the lowest-lying level is defined by the

Table 1
Summary of geometric features of the M_2Si_n clusters considered. HP and AHP stand for hexagonal prism and hexagonal anti-prism, respectively.

Cluster size	Nb_2Si_n	Mo_2Si_n	$MoNbSi_n$	Ta_2Si_n	W_2Si_n	$TaWSi_n$
11	Tube	Tube	Tube	Tube	Tube	Tube
12	HP	AHP	HP + AHP	HP	AHP	HP + AHP
13	Tube	Tube	Tube	Tube	Tube	Tube
14	Cage	Tube	Tube + cage	Cage	Tube	Tube
15	Cage	Cage	Cage	Cage	Cage	Cage
16	Cage	Tube	Tube	Cage	Cage	Cage
17	Cage	Fused cage	Cage	Cage	Fused cage	Cage
18	Fused cage	Fused cage	Fused cage	Fused cage	Fused cage	Fused cage

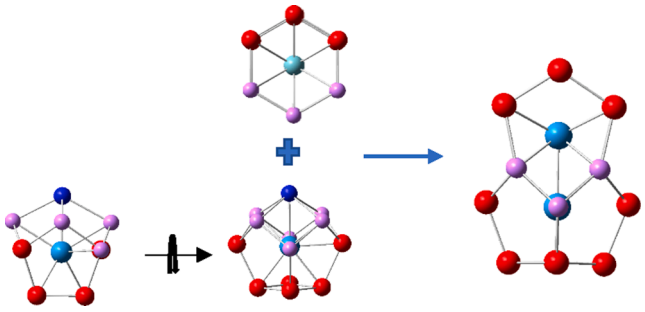

Fig. 5. The fusion mechanism of two cages leading to the M_2Si_{18} fused cage.

Table 2
M–M bond length (Å) and NBO net charges (au) of metal atom(s) in clusters at different Si sizes.

Structure	$d_{(M-M)}$	NBO charge (inner; outer)	Structure	$d_{(M-M)}$	NBO charge (inner; outer)
Nb2.11.A	2.56	−2.4; −1.0	**Nb2.15.A**	3.11	−3.7;−1.2
Mo2.11.A	2.34	−2.6;−1.1	**Mo2.15.A**	3.13	−3.7;−1.5
Ta2.11.A	2.54	−2.5; −0.8	**Ta2.15.A**	3.06	−3.5;−1.2
W2.11.A	2.43	−3.4;−1.0	**W2.15.A**	2.50	−3.2; −1.45
NbMo.11.A	2.43	−2.8; −0.7	**NbMo.15.A**	3.21	−3. 7;−1,12
TaW.11.A	2.42	−2.7;−0.6	**TaW.15.A**	3.21	−3.5;−1.1
Nb2.12.A	2.5	−0.7;−3.6	**Nb2.16.A**	3.28	−3.7;−0.9
Mo2.12.A	2.3	−1.0;−3.4	**Mo2.16.A**	2.42	−3.3;−2.5
NbMo.12.A	2.4	−0.6;−3.6	**Ta2.16.A**	2.78	−3.3;−1.0
Ta2.12.A	2.5	−0.7;−3.3	**W2.16.A**	2.56	−2.9;−2.1
W2.12.A	2.4	−1.0;−3.3	**NbMo.16.A**	2.48	−3. 5;−2.4
TaW.12.A	2.5	−0.6; −3.5	**TaW.16.A**	2.69	−3. 5;−1.2
Nb2.13.A	2.54	−3.7;−0.8	**Nb2.17.A**	3.19	−3.8;−1.9
Mo2.13.A	2.38	−3.5;−1.4	**Mo2.17.A**	2.56	−3.5;−2.9
Ta2.13.A	2.56	−3.5;−1.0	**Ta2.17.A**	3.28	−3.7;−2.3
W2.13.A	2.41	−3.4;−1.4	**W2.17.A**	2.59	−3.4;−2.9
NbMo.13.A	2.47	−3.6;−1.1	**NbMo.17.A**	2.71	−3.6;−2.3
TaW.13.A	2.50	−3.5;−1.1	**TaW.17.A**	2.69	−3.5;−2.3
Nb2.14.A	3.14	−3.8;−0.8	**Nb2.18.A**	2.54	−3.2;−2.9
Mo2.14.A	2.40	−3.2;−1.7	**Mo2.18.A**	2.52	−3.5;−3.0
Ta2.14.A	3.10	−3.5;−0.8	**Ta2.18.A**	2.60	−3.2;−2.8
W2.14.A	2.50	−3.2;−1.6	**W2.18.A**	2.55	−3.5;−2.9
NbMo.14.A	3.22	−3.7;−0.7	**NbMo.18.B**	2.58	−3.4;−3.0
TaW.14.A	2.58	−3.3;−1.3	**TaW.18.A**	2.70	−3.5;−2.3

principle number N = 1. In this electron shell model, a successive occupation of a level, giving rise to a corresponding magic number such as 2, 8, 20, (34), 40,… could lead to a thermodynamically stable cluster.

Saillard et al. [44] recently analyzed the stability of fused clusters under the view of the electron shell model. These authors showed that the establishment of a fused structure is associated with a closed electronic shell. As for a representative case, Fig. 6 displays the total density of state (DOS) and partial density of state (pDOS) of Mo_2Si_{18} and Nb_2Si_{18} fused clusters. The DOS maps of other fused clusters are given in Figs. S11, S12, S13 and S14 of the ESI file. The DOS of Nb_2Si_{18} show that the 1S, 2S, 1P, 2P, 1D, 2D, 1F and 1G levels are fulfilled while the 1H eigenstates are occupied by 14 electrons and end up with a configuration of $[1S^2\ 1P^6\ 1D^{10}\ 1F^{14}\ 1G^{18}\ 1H^{14}\ 2S^2\ 2P^6\ 2D^{10}]$, which is populated by 82 valence electrons. The same electron configuration also found for Ta_2Si_{18} fused cluster (Fig. S12 of ESI). Similarly, the entire set of 84 valence electrons of the Mo_2Si_{18} and W_2Si_{18} fused clusters populate a shell structure of $[1S^2\ 1P^6\ 1D^{10}\ 1F^{14}\ 1G^{18}\ 1H^{16}\ 2S^2\ 2P^6\ 2D^{10}]$. The main difference between these two series concerns the occupancy of the 1H subshell, namely, 14 electrons in the former and 16 electrons in the latter. The mixed $MoNbSi_{18}$ and $TaWSi_{18}$ systems share a configuration of $[1S^2\ 1P^6\ 1D^{10}\ 1F^{14}\ 1G^{18}\ 1H^{17}\ 2S^2\ 2P^6\ 2D^{10}]$ as shown in Fig. S11 and S14 of ESI. Accordingly, the high stability of M_2Si_{18} fused clusters can be rationalized in terms of emergence and complete occupancy of a characteristic electron shell pattern by the whole set of valence electrons.

4. Concluding remarks

We present in this theoretical paper the geometry and stability features of the doubly metal doped silicon clusters M_2Si_n with M_2 = Mo_2, Nb_2, Ta_2, W_2, NbMo, TaW and n = 11–18. Geometric structures of the M_2-doped silicon clusters within this range of sizes tend to change from a tubular shape to a cage and then a fussed cage. Geometries of the smaller M_2Si_{11}, M_2Si_{12} and M_2Si_{13} clusters show a predominance of a tube; in the size range n = 14–18 a structural transition occurs from a tube to a singly doped cage and then a fused cage. The M_2Si_{18} block presents a novel structural motif, namely the fused cage, for silicon clusters. Each M_2Si_{18} fused cage arises from a fusion of the $M@Si_{10}$ and $M@Si_{12}$ prisms followed by addition of two Si atoms. Formation and occupancy of electron shells contribute to the high thermodynamic stability of the M_2Si_{18} fused clusters. We would hope that the beauty of this structural motif could motivate experimental studies on silicon fused cages.

Funding Information

This research was funded by Ho Chi Minh City's Department of Science and Technology (HCMC-DOST) and Institute for Computational Science and Technology (ICST) under grant number 43/2020/HĐ-QPTKHCN.

CRediT authorship contribution statement

Hung Tan Pham: Conceptualization, Data curation, Formal analysis, Funding acquisition, Writing – original draft, review & editing. **Cam-Tu Phan Dang:** Data curation, Formal analysis. **Long Van Duong:** Data curation, Formal analysis. **Phan Toai Tuyn:** Data curation, Formal analysis. **Minh Tho Nguyen:** Conceptualization, Supervision, Validation, Writing – review & editing.

Declaration of Competing Interest

The authors declare that they have no known competing financial interests or personal relationships that could have appeared to influence the work reported in this paper.

Appendix A. Supplementary material

Figures display shapes and relative energies of the lower-lying isomers of different sizes and metal dopants their growth patterns and density of states plots. To assist a further experimental study, the

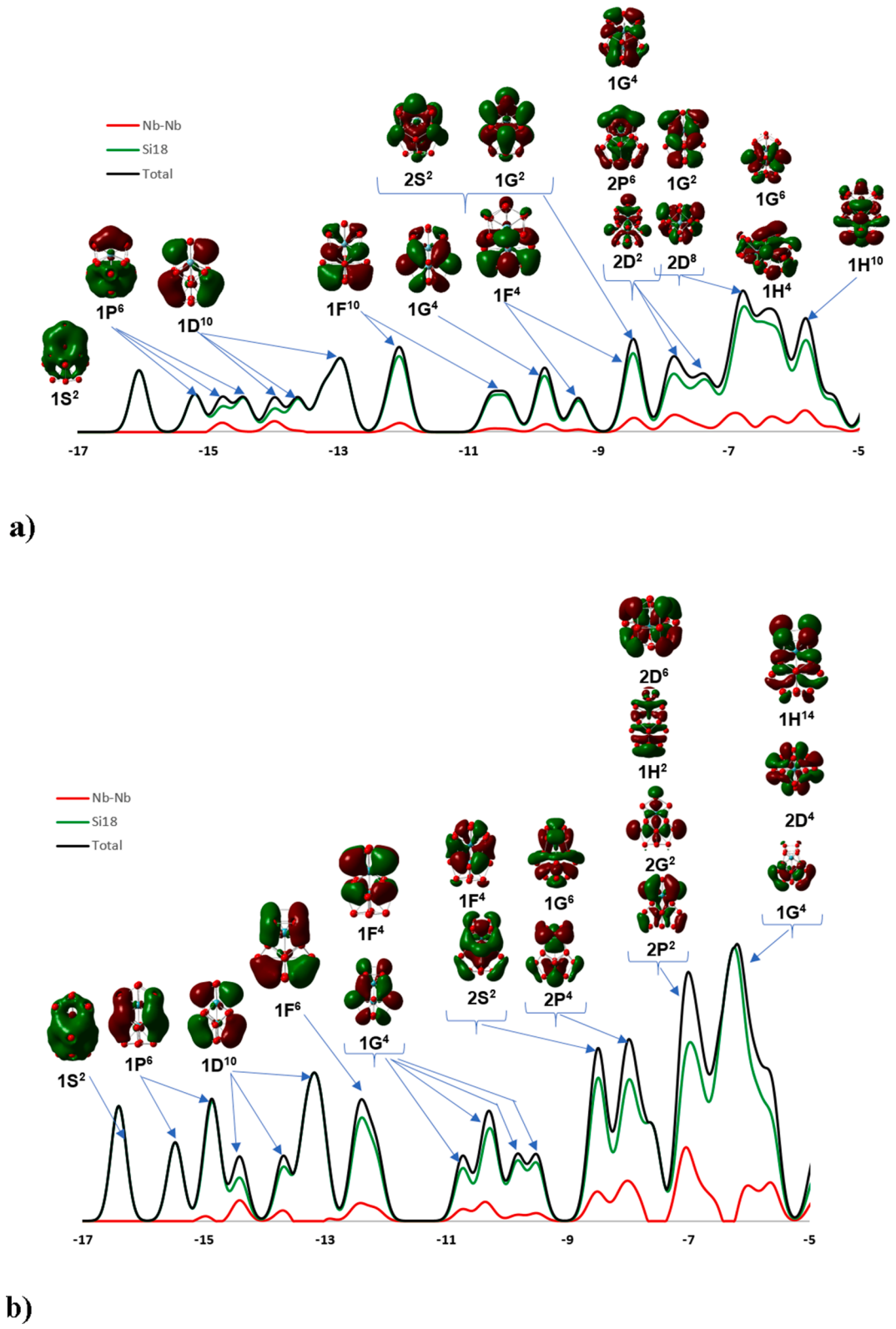

Fig. 6. Plots of density of states of **a)** Nb_2Si_{18} and **b)** Mo_2Si_{18} fused clusters.

predicted IR spectra of the most stable isomer(s) of the lowest-lying isomers M_2Si_n are also displayed. Supplementary data to this article can be found online at https://doi.org/10.1016/j.cplett.2021.139229.

References

[1] W.L. Brown, R.R. Freeman, K. Raghavachari, M. Schluter, Science 235 (1987) 860.
[2] E.C. Honea, A. Ogura, C.A. Murray, K. Raghavachari, W.O. Sprenger, M.F. Jarrold, W.L. Brown, Nature 366 (1993) 42.
[3] Y. Kamata, Mater. Today 11 (2008) 30.
[4] R. Pillarisetty, Nature 479 (2011) 324.

[5] G. Pacchioni, J. Koutecký, J. Chem. Phys. 84 (1986) 3301.
[6] N. Veldeman, P. Gruene, A. Fielicke, P. Claes, V.T. Ngan, M. T. Nguyen, P. Lievens, in: K.D. Sattler (Ed.), Handbook of Clusters, CRC Press, Boca Raton, FL, USA, 2010, Chapter 5.
[7] O. Cheshnovsky, S.H. Yang, C.L. Pettiette, M.J. Craycraft, Y. Liu, R.E. Smalley, Chem. Phys. Lett. 138 (1987) 119.
[8] U. Röthlisberger, W. Andreoni, M. Parrinello, Phys. Rev. Lett. 72 (1994) 665.
[9] N.M. Tam, H.T. Pham, M.T. Nguyen, Chem. Phys. Lett. 608 (2014) 255.
[10] S. Li, R.J. Van Zee, W. Weltner, K. Raghvachari, Chem. Phys. Lett. 243 (1995) 275.
[11] K.M. Ho, A.A. Shvartsburg, B. Pan, Z.Y. Lu, C.Z. Wang, J.G. Wacker, J.L. Fye, W. L. Brown, Nature 392 (1998) 582.
[12] A.A. Shvartsburg, B. Liu, M.F. Jarrold, K.M. Ho, J. Chem. Phys. 112 (2000) 4517.
[13] W. Hellmann, R.G. Hennig, S. Goedecker, C.J. Umrigar, B. Delley, T. Lenosky, Phys. Rev. B 75 (2007) 085411.
[14] S.M. Beck, J. Chem. Phys. 87 (1987) 4233.
[15] M. Haertelt, J.T. Lyon, P. Claes, J. de Haeck, P. Lievens, A. Fielicke, J. Chem. Phys. 136 (2012) 064301.
[16] M.I.A. Oliveira, R. Rivelino, F. de Brito Mota, G.K. Gueorguiev, J. Phys. Chem. C 118 (2014) 5501.
[17] F. Hagelberg, C. Xiao, Phys. Rev. B 67 (2003) 035426.
[18] N. Uchida, T. Miyazaki, T. Kanayama, Phys. Rev. B 74 (2006) 205427.
[19] M.B. Abreu, A.C. Reber, S.N. Khanna, J. Phys. Chem. Lett. 5 (2014) 3492.
[20] K. Koyasu, M. Akutsu, M. Mitsui, A. Nakajima, J. Am. Chem. Soc. 127 (14) (2005) 4998.
[21] J.U. Reveles, S.N. Khanna, Phys. Rev. B 74 (2006) 035435.
[22] Z. Liu, X. Wang, J. Cai, H. Zhu, J. Phys. Chem. C 119 (2015) 1517.
[23] T. Iwasa, A. Nakajima, J. Phys. Chem. C 116 (2012) 14071.
[24] H.T. Pham, D. Majumdar, J. Leszczynski, M.T. Nguyen, Phys. Chem. Chem. Phys. 19 (2017) 3115.
[25] S.J. Lu, H.G. Xu, X.L. Xu, W.J. Zheng, J. Phys. Chem. C 121 (2017) 11851.
[26] X. Huang, S.J. Lu, X. Liang, Y. Su, L. Sai, Z.-G. Zhang, J. Zhao, H.-G. Xu, W. Zheng, J. Phys. Chem. C 119 (2015) 10987.
[27] H.T. Pham, D.T.T. Mai, L.V. Duong, N.M. Tam, M.T. Nguyen, Phys. Chem. Chem. Phys. 20 (2018) 7588–7592.
[28] H.T. Pham, H.G. Rizzo, R.W.A. Havenith, M.T. Nguyen, J. Phys. Chem. C 123 (40) (2019) 24676.
[29] H.T. Pham, T.T. Phan, N.M. Tam, L.V. Duong, M.P. Pham-Ho, M.T. Nguyen, Phys. Chem. Chem. Phys. 17 (2015) 17566.
[30] W. Ji, C. Luo, Int. J. Quantum Chem. 112 (2012) 2525.
[31] H.T. Pham, L.V. Duong, P.Q. Buu, M.T. Nguyen, Chem. Phys. Lett. 577 (2013) 32.
[32] J.M. Tao, J.P. Perdew, V.N. Staroverov, G.E. Scuseria, Phys. Rev. Lett. 91 (2003) 146401.
[33] A.D. Becke, J. Chem. Phys. 98 (1993) 5648.
[34] V.T. Ngan, K. Pierloot, M.T. Nguyen, Phys. Chem. Chem. Phys. 15 (2013) 5493.
[35] M.S. Gordon, J.S. Binkley, J.A. Pople, W.J. Pietro, W.J. Hehre, J. Am. Chem. Soc. 104 (1983) 2797.
[36] K.D. Dobbs, W.J. Hehre, J. Comput. Chem. 8 (1987) 861.
[37] K. Raghavachari, J.S. Binkley, R. Seeger, J.A. Pople, J. Chem. Phys. 72 (1980) 650.
[38] P.J. Hay, J. Chem. Phys. 66 (1977) 4377.
[39] A.E. Reed, L.A. Curtiss, F. Weinhold, Chem. Rev. 88 (1988) 899.
[40] M.J. Frisch, H.B. Schlegel, G.E. Scuseria, M.A. Robb, J.R. Cheeseman, J.A. Montgomery, T. Vreven, K.N. Kudin, J.C. Burant, J. Millam, et al., Gaussian 09 Revision: B.01; Gaussian, Inc.: Wallingford, CT, 2009.
[41] Z.M. Sun, H. Xiao, J. Li, L.S. Wang, J. Am. Chem. Soc. 129 (31) (2007) 9560.
[42] F.K. Sheong, W.J. Chen, J.X. Zhang, Y. Li, Z. Lin, Dalton Trans. 46 (2017) 2214.
[43] M. Brack, Rev. Mod. Phys. 65 (1993) 67.
[44] F. Gam, C.W. Liu, S. Kahlala, J.Y. Saillard, Nanoscale 12 (2020) 20308.